Structure and charge transport anisotropy of polythieno[3,4- b]-thiophene- co -benzodithiophene (PTB7) oriented by high-temperature rubbing

Laure Biniek, Amer Hamidi-Sakr, Linda Grodd, Stéphanie Escoubas, Yannick Dappe, Souren Grigorian, Marc Schmutz, Martin Brinkmann

Structure and charge transport anisotropy of polythieno[3,4-*b*]-thiophene-co-benzodithiophene (PTB7) oriented by high-temperature rubbing.

Laure Biniek[1+], Amer Hamidi-Sakr[1+], Linda Grodd [2], Stéphanie Escoubas[4], Yannick J.Dappe[3]

Souren Grigorian[2], Marc Schmutz[1], Martin Brinkmann[1]*

(1) Université de Strasbourg, CNRS, ICS UPR 22, F-67000 Strasbourg, France

(2) Department of Physics, University of Siegen, Walter Flex Strasse-3, D-57068 Siegen, Germany

(3) SPEC, CEA, CNRS, Université Paris-Saclay, CEA Saclay, 91191 Gif-sur-Yvette Cedex, France

(4) Aix-Marseille Université, IM2NP, Faculté des Sciences et Techniques, Avenue Escadrille Normandie Niemen - Case 142, F-13397 Marseille, France

Corresponding author: martin.brinkmann@ics-cnrs.unistra.fr

+ : Both authors contributed equally to this work

Figure for Table of content

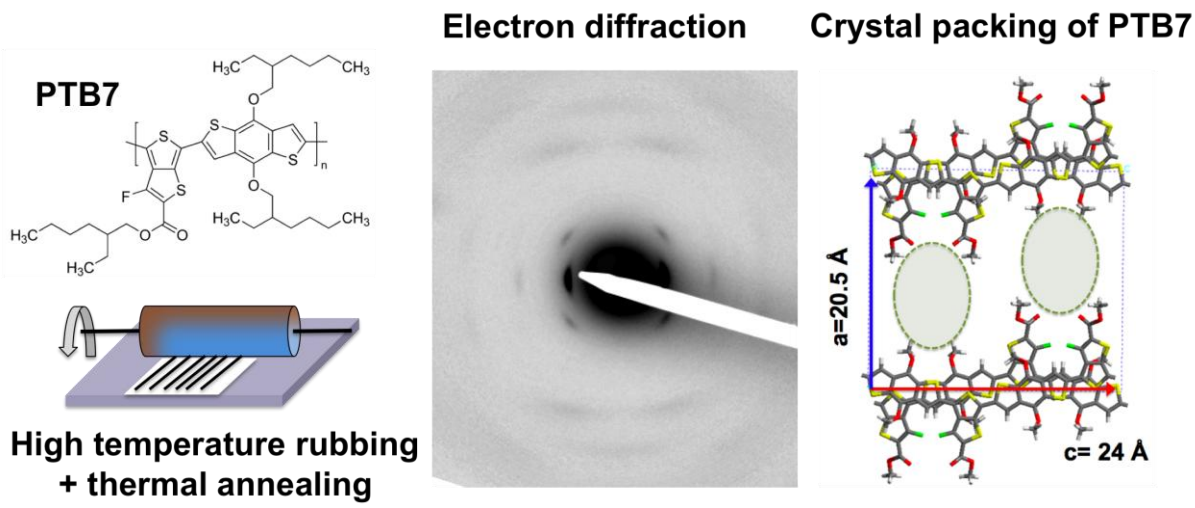

Summary

Combining high temperature rubbing and isothermal crystallization affords oriented films of the polymer semiconductor PTB7 with high dichroic ratio and anisotropic hole mobilities. Structural analysis yields three possible models that share similar structural features: a layered packing with strongly interdigitated side chains, a non-planar zig-zag backbone conformation and a mixed stacking of thieno[3,4-*b*]thiophene and benzodithiophene blocks.

Abstract

Structure determination in high performance polymer semiconductors such as polythieno[3,4-*b*]-thiophene-co-benzodithiophene (PTB7) is essential to establish proper structure-property correlations. A combination of high temperature rubbing and isothermal crystallization leads to oriented and crystalline films of face-on oriented PTB7 crystals. Electron diffraction (ED) indicates that crystallinity is marginal in the rubbed films but develops upon post-rubbing annealing at T≥250°C. The best oriented and crystalline PTB7 films have a dichroic ratio of 12 for the UV-vis absorption. The hole mobilities are improved by a factor of six along the rubbing direction over non-aligned films ($\mu_{//}$= 5.8 x10^{-3} cm^2/V.s versus $\mu_{\perp}$=3.1 x10^{-4} cm^2/V·s). Structural analysis yields three possible models that however share similar structural features, namely i) PTB7 chains form a layered packing such as PBTTT with π-stacked backbones alternating with layers of strongly interdigitated alkyl side chains, ii) the PTB7 chains adopt a non-planar zig-zag conformation, iii) PTB7 chains show a mixed stacking of thieno[3,4-*b*]thiophene and benzodithiophene blocks. Overall, these results highlight the key role played in polymer semiconductor crystals by the steric constraints due to the branched alkyl side chains interdigitation on the π-stacking of conjugated backbones.

1. Introduction.

Mastering morphology and crystallinity of polymer semi-conductors (PSCs) is essential to control device properties in organic field effect transistors (OFETs) and organic photovoltaics (OPV).[1] Most conjugated polymers are semi-crystalline i.e. both amorphous and crystalline domains coexist in thin films.[2] Some of the recently investigated high performance PSCs have low crystallinity in thin films and were regarded as "semi-amorphous" despite relatively high charge mobilities.[3] However, the processing conditions yielding active layers in thin films are usually far from equilibrium and do not allow to reach the highest possible crystallinity. Specific nucleation and growth conditions e.g. via self-seeding are usually required to grow single crystals or multilamellar objects such as spherullites.[4] Several alternative ways can enforce crystallinity by favoring the nucleation of the polymers: self-seeding, use of nucleating agents such as carbon nanotubes[5] or self-assembled nanofibrils of sorbitol-derivatives,[6] nucleating surfaces to promote epitaxy of polymer crystals[7-10] or application of shear forces to align polymer chains.[11-14] On the one hand, preferred orientation and crystallization is readily achieved by epitaxy on the surface of polymers or molecular crystals. Directional epitaxial crystallization of PSCs helped to crystallize and orient important PSCs e.g. regioregular poly(3-hexylthiophene) (P3HT), poly(di-*n*-octylfluorene) (PFO) and poly{[N,N´-bis(2-octyldodecyl)-1,4,5,8-naphthalenedicarboximide-2,6-diyl]-alt-5,5´-(2,2´-bithiophene)} (P(NDI2OD-T2)).[2,7-10] On the other hand, shear forces generate bundles of highly oriented chains that can subsequently act as oriented seeds for the crystallization of the polymer. One such alignment method based on shear is high-temperature rubbing.[11-15] A rotating cylinder

covered with a cloth helps align polymer chains when applied on a thin film. The temperature of the film used during rubbing is crucial. It depends on the molecular weight distribution of the polymer, as demonstrated recently for various PSCs. Low molecular weight fractions of P3HT are readily oriented at room temperature whereas high-M_w fractions are not.[13] Instead, when rubbing is performed at T>150°C, highly oriented and crystalline films of P3HT with M_w=50kDa were obtained.[15] Increasing the temperature of rubbing actually helps disentangle polymer chains when the alkyl side chains are molten.[13] This strategy was used successfully to refine the crystal packing of two chemically complex PSCs, namely poly{[4,4-bis(2-ethylhexyl)-cyclopenta-(2,1-b;3,4-b')dithiophen]-2,6-diyl-*alt*-(2,1,3-benzothiadiazol)-4,7-diyl} (PCPDTBT) and poly{[4,4-bis(2-ethylhexyl)-cyclopenta-(2,1-b;3,4-b')dithiophen]-2,6-diyl-*alt*-(5-fluoro-2,1,3-benzothiadiazol)-4,7-diyl} (F-PCPDTBT).[16] Herein, high temperature rubbing is applied to Poly[[4,8-bis[(2-ethylhexyl)oxy]benzo[1,2-*b*:4,5-*b*']dithiophene-2,6-diyl-[3-fluoro-2-[(2-ethylhexyl)carbonyl]thieno[3,4-*b*]thiophene-4,6-diyl]], namely PTB7 (see Figure 1.a).

PTB7 derivatives are very promising electron donor materials for organic photovoltaic applications. Solar cells with power conversion efficiencies in excess of 9% have been reported.[17-19] The domain size of PTB7 derivatives blended with [6,6]-phenyl-C_{61}-methylbutanoate (PCBM) is usually controlled through the use of solvent additive.[20-25] As-cast films of pure PTB7 and blends have a low crystallinity (20%) with a majority of face-on orientation of polymer chains in the crystalline domains. The crystallization and the structure of PTB7 are not known in detail. In most studies, only two reflections corresponding to a 19 Å inter-layer stacking and a π-stacking periodicity of 3.9 Å were observed in grazing incidence X-ray diffraction data and the polymer was reported to π-

stack in a layered structure similar to that observed for P3HT.[22,23] The exact chain conformation or the way of stacking of the chains could not be determined from the limited structural data.

This study reports the preparation of highly oriented films of PTB7 using high temperature rubbing followed by post-rubbing annealing. For optimal crystallization conditions, well defined diffraction patterns are obtained and help refine the structure of the polymer. Charge transport anisotropy was also determined in OFETs from rubbed thin films (Figure 1.b and 1.c) and for the optimal alignment/crystallization conditions, hole mobilities are observed to be six-times the values of non-aligned PTB7 films.

2. Results.

2.1. Alignment of PTB7, impact of rubbing temperature and annealing on orientation, UV-vis absorption and anisotropy of charge mobility.

a) Alignment versus rubbing temperature.

Thin films of PTB7 were prepared by doctor blading a 5 wt% solution in *ortho*-dichlorobenzene (*o*DCB) at 170°C or in chloroform (CF) at 53°C on clean glass substrates and subsequently rubbed at various temperatures in a glovebox. A particular attention has been paid on the samples (and devices) preparation in a controlled atmosphere since the PTB7 films have limited stability in air. As seen in Figure 1.b and 1.c, the rubbed films are highly birefringent in the Polarized Optical Microscope (POM), indicating significant alignment upon rubbing with limited surface roughness as indicated by Scanning Electron Microscopy (Figure S1). Alignment is confirmed by UV-Vis polarized absorption spectroscopy (see Figure 1.d and 1.e). Figure 1.d depicts the UV-Vis spectrum of the PTB7 films rubbed at 150°C. It shows a vibronic structure with a

0-0 component at 670 nm and a 0-1 at 610 nm (Figure 1.d and 1.e). Maximum absorbance is observed when the incident light is polarized parallel to the rubbing direction, indicating that PTB7 chains align parallel to the rubbing direction. No important shifts of the spectra are observed with rubbing temperature and the 0-0/0-1 intensity ratio is also relatively constant. As observed for other PSCs, the alignment improves with increasing rubbing temperature up to 200°C with dichroic ratio $DR=A_{//}/A_{\perp}$ ~5-6 (see Figure 1.f and 1.g). The structure of these rubbed films was observed by Transmission Electron Microscopy (TEM). All rubbed films show marginal traces of order in the electron diffraction patterns that consist of a single equatorial reflection at 2.1 nm corresponding to the distance between layers of PTB7 chains separated by the alkyl side chains. The absence of reflection corresponding to the in-plane π-stacking periodicity indicates that rubbed PTB7 films consist of face-on domains, as observed for numerous PSCs upon rubbing.[12-15] Bright field TEM shows almost featureless morphology with no evidence of lamellar crystals. Clearly, high-T rubbing does align PTB7 chains parallel to the rubbing direction but does not allow the chains to crystallize efficiently.

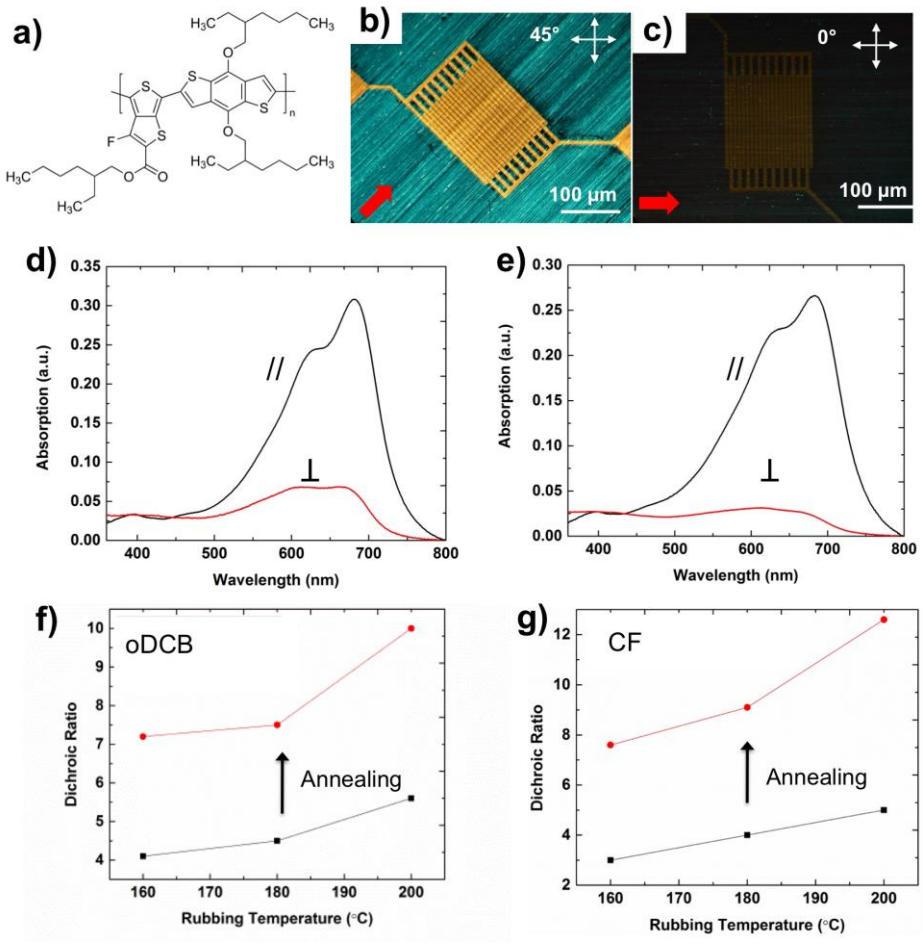

***Figure 1**. a) Chemical structure of PTB7. (b) & (c)Polarized optical microscopy image (at 45° and 0° orientation with respect to the polarization of the incident light) showing the high birefringence of a rubbed OFET device (T_R=200°C). The red arrow indicates the direction of rubbing. (d) Polarized UV-Vis absorption spectra of oriented PTB7 films deposited from CF and rubbed at 200°C and (e) subsequently annealed at 260°C for one hour. The spectra were recorded for the incident polarization parallel to the rubbing direction (//) or perpendicular (⊥). (f) and (g) Evolution of the dichroic ratio as a function of rubbing temperature before (black symbols) and after annealing (red symbols) of the rubbed films at 260°C (1 hr) for PTB7 films prepared by doctor blading in oDCB (f) and in chloroform (CF) (g).*

b) Impact of thermal annealing on rubbed PTB7 films.

In order to improve orientation and crystallinity, the rubbed samples were subjected to thermal annealing at different temperatures T_A. As seen in Figure 1.f and 1.g, polarized absorption spectroscopy reveals an increase of the dichroic ratio DR for all rubbed films after annealing at 260°C for one hour. The orientation improves even for short annealing periods of a 5 minutes (see Figure S2). As an example, a 150°C-rubbed PTB7 film shows an increase of DR from 3.5 to 8.8 after annealing at 260°C for 5 min. Increasing further the annealing period to one hour improves only slightly the dichroic ratio (10.3 for 5 min to 12.6 for one hour). The best alignment (DR=12.6) was observed for PTB7 films prepared from solutions in chloroform (CF) after rubbing at 200°C and thermal annealing for 1 hour at 260°C (Figure 1.g). Such annealing does not alter substantially the vibronic structure of the absorption spectra (the amplitude ratii $A_{0\text{-}0}/A_{0\text{-}1}$ between the 0-0 and 0-1 components shows a small decrease from 1.25 to 1.15 after annealing).

As a matter of fact, combining high rubbing temperatures of 240°C and high annealing temperature impacts the contact plane of the aligned PTB7 crystals in the films. For T_R=240°C and T_A=260°C-270°C (below the melting temperature), the initial majority of face-on oriented domains is maintained after annealing. In contrast, for T_A=290°C the films consist mainly of edge-on oriented domains as indicated by a strong equatorial "π-stacking" reflection at 3.75 Å (see supporting figure S3).

Most interestingly, the choice of the solvent used for doctor blading of the films prior to rubbing is found to impact the final structure of the rubbed films after isothermal crystallization at 260°C. Rubbed oDCB-films of PTB7 show no substantial structural changes after annealing: the strength of the 1 0 0 equatorial reflection

remains unchanged despite the improved alignment evidenced by the increased dichroic ratio (see Figure 1.f).

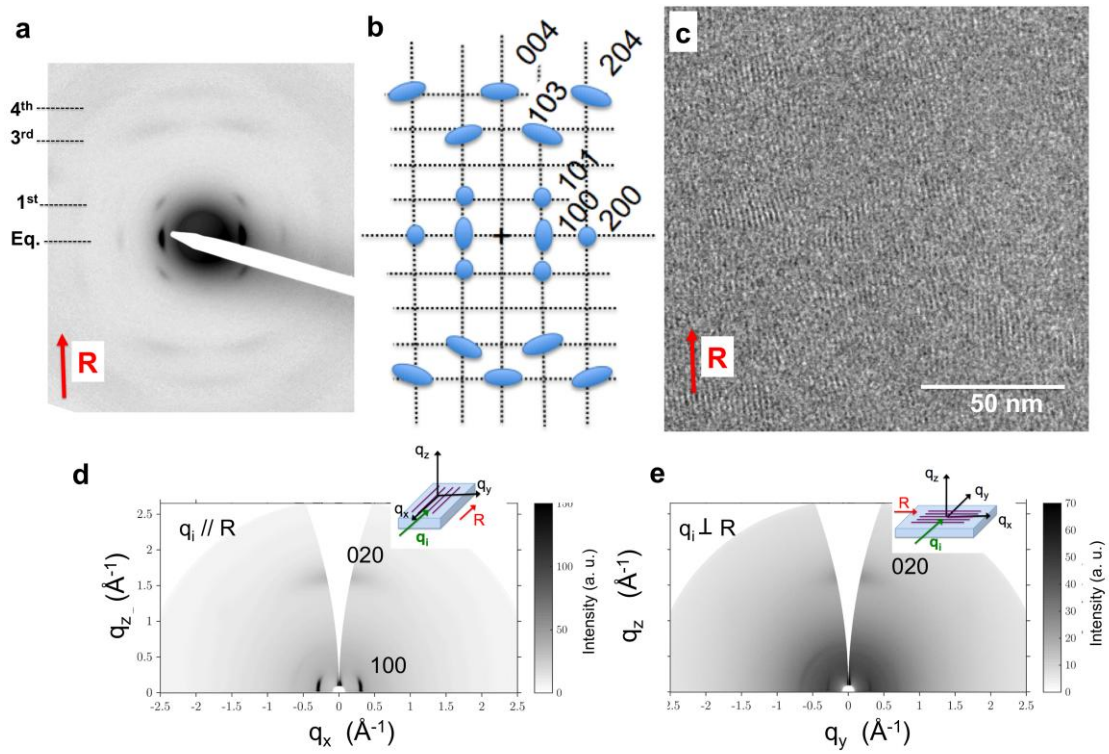

Figure 2*. a) Experimental (a) and schematic view (b) of the electron diffraction pattern for PTB7 films oriented by high-temperature rubbing at 200°C followed by isothermal crystallization at 260°C for one hour. In (a), the arrow points at the direction of rubbing (chain direction of PTB7). (c) HRTEM image showing the semi-crystalline structure of the PTB7 films. (d) and (e) GIXD patterns of the oriented PTB7 films recorded for the incident X-ray beam oriented parallel (d) and perpendicular (e) to the rubbing direction R.*

This is in strong contrast to the rubbed CF-films that show a marked change of crystallinity after 260°C-annealing. Indeed, as seen in Figure 2.a, the characteristic Electron Diffraction (ED) pattern of the rubbed CF-films show numerous reflections including mixed index reflections that indicate improved crystallinity after annealing. The impact of the solvent used to doctor blade PSC films on the level of alignment was

previously reported for PFO thin films.[13] It was proposed that the efficient orientation of polymer chains by rubbing occurs more readily for thin films, the structure of which is more amorphous prior to rubbing.

c) Crystalline and lamellar organization of thin films.

The reflections in the ED pattern of Figure 2.a can be indexed by considering a dominant contact plane corresponding to face-on crystals only, consistent with the High Resolution TEM (HRTEM) images of such films (see Figure 2.c). This orientation is further confirmed by the appearance of the 0.37-0.38 nm π-stacking reflection when the sample is tilted by 60° around the rubbing direction (chain direction). In an attempt to quantify the amount of ordered face-on domains in such films, we have measured the relative area occupied by ordered domains in the HRTEM images. It turns out that 20-25% of the surface of HRTEM images is covered by face-on domains that represent the major contribution in the ED pattern (a minor proportion of edge-on domains is also present in this sample). Hence, a lower bound for the crystallinity in PTB7 might be 20-25%. As compared to regioregular poly(3-hexylthiophene) that can show up to 50-60% crystallinity, the crystallinity in PTB7 is remarkably low.[15] Grazing Incidence X-ray Diffraction (GIXD) data are also consistent with this observation and reveals a pronounced anisotropy of the diffraction patterns along and across to the rubbing direction. The 0 2 0 π-stacking reflection is located along the substrate normal (out-of-plane) whereas the 1 0 0 reflection is observed in-plane for an incident X-ray beam parallel to the rubbing direction (q_i//R) (see Figure 2.d and 2.e). The structure of PTB7 is thus a layered structure similar to that of P3HT form I or poly(2,5-bis(3-dodecyl-2-yl)thieno[3,2-*b*]thiophene) (PBTTT). Following the convention of unit cell axes used in P3HT, the **a, b** and **c** axes are along the side chains, the π-stacking and the chain

directions, respectively. Accordingly, all reflections in the ED of Figure 2.a are indexed as h 0 ℓ reflections (see Figure 2.b). The fact that some reflections are observed along the chain direction up to the 9th layer line indicates that there can be both substantial conformational and stacking order of the backbones in this type of PSC. However, the limited number of reflections and their weak intensities suggest that alkyl side chains are highly disordered, as compared for instance to regioregular poly(3-(2,5-dioctylphenyl)thiophene) (PDOPT) or poly(dioctylfluorene).[7] From a morphological point of view, while no obvious lamellar structure is evident in the bright field images, evidence for semi-crystallinity is obtained by low dose HRTEM. As seen in Figure 2.c, the HRTEM images of rubbed and annealed PTB7 films exhibit well defined face-on nanocrystals identified by their typical fringed patterns with a 2.1 nm periodicity which is in good agreement with GIXD measurements. Such HRTEM images also show that PTB7 has a semi-crystalline morphology with coexisting crystalline and amorphous domains.

d) Charge transport versus rubbing and annealing.

The impact of crystallinity and alignment on charge transport was investigated by using the oriented films of PTB7 as semi-conducting layers in Organic Field Effect Transistors (OFETs). The PTB7 films were spin-coated, rubbed at 200°C and subsequently annealed at either 260°C or 290°C on hexamethylsilazane (HMDS) treated bottom gate – bottom contact (BG-BC) devices in a glovebox (260°C corresponds to the best observed DR of the films). OFETs were characterized both along and normal to the rubbing direction to extract the corresponding mobilities $\mu_{//}$ and $\mu_{\perp}$, respectively. The non-oriented spin-coated films exhibit a hole mobility of 9.6±0.4 x10^{-4} cm^2/V·s after annealing at 260°C which is slightly larger than the value reported by Xu et al. (6 x10^{-4}

$cm^2/V.s$ for a non-annealed TG-BC device configuration).[26] Figure S4 shows typical transfer and output characteristics of the samples rubbed and annealed at 260°C. Table S1 collects the extracted OFET parameters. The samples rubbed and annealed show a high hole mobility parallel to the rubbing direction with $\mu_{//}$= 5.8±0.4 x10^{-3} $cm^2/V{\cdot}s$. The average mobility values determined in the perpendicular direction are $\mu_{\perp}$=3.1±0.9 x10^{-4} $cm^2/V{\cdot}s$. Accordingly, the PTB7 films with improved crystallinity and dominant face-on contact plane show substantially improved charge mobilities compared to the non-aligned films, underlining the higher charge transport along the chain direction over transport along the insulating side chains. The observed charge transport anisotropy $\mu_{//}/\mu_{\perp}$ = 18±3 is similar to that observed in rubbed films of other polymer semiconductors such as P3HT, PBTTT or p(NDI2OD-T2).[14,15, 27] The mobility anisotropy exceeds the value of the dichroic ratio DR for UV-vis absorption (8-10). This observation is explained by the fact that both anisotropy factors refer to different physical properties. On one side, the dichroic ratio DR quantifies the orientation distribution of polymer chains in the film plane along the rubbing direction. On the other side, the macroscopic charge transport anisotropy $\mu_{//}/\mu_{\perp}$ probed in OFETs depends on both the crystal orientation distribution and the intrinsic charge transport anisotropy μ_a/μ_c of face-on domains (μ_a and μ_c are the charge mobilities along the side chain and the backbone, respectively). In face-on crystals of PTB7, charge transport is most presumably very low along the insulating side chains as compared to the backbone direction. This should lead to high anisotropies μ_a/μ_c, hence to high macroscopic charge transport anisotropies $\mu_{//}/\mu_{\perp}$ in transistors.

2.2. Structure of PTB7.

a) Description of structural models.

The methodology used to refine the structure of PTB7 is described in detail in the supplementary information. Three possible structures that reproduce best the experimental ED (two structures with a P21/c space group, labelled Model1 and Model2 and one model with P21 symmetry labelled Model 3) were identified using a zig-zag backbone conformation optimized by DFT calculations.[25] Figure 3 gathers the calculated ED patterns (Figure 3.a and 3.d) and the projections of the two structures with P21/c space group along the π-stacking direction (3.b and 3.e) and the chain direction (3.c and 3.f). For clarity, a schematic illustration of the two models is also shown in Figure 3.b and 3.e to highlight the different chain overlaps in the models (benzodithiophene (thienothiophene) is represented by a blue (orange) rectangle). As a matter of fact, the two models differ mainly by the relative shift between the chains along the chain direction Δc. Model 1 and Model 2 correspond to Δc=-7.5 Å and Δc=+6.1Å, respectively (Δc is positive in the c axis direction). Most importantly, the shift between the chains along the chain direction Δc is the result of the steric constraints between the branched alkyl side chains of the thieno[3,4-*b*]thiophene blocks that impede a perfect segregated stacking (see Figure S5).

In the P21/c space group (Model 1 and 2), two PTB7 chains are π-stacked along **b** and their bulky side chains are grouped together alternatively along **a** and –**a** at a periodicity of c/2. This packing leads to an effective interdigitation of side chains that is perfectly adapted to the zig-zag conformation of the PTB7 backbone: the side groups of one stack of chains are located in the voids left by the next stack of chains along **a.** The bulky branched alkyl side chains segregate from the backbones and are located in the

voids highlighted by light grey ellipses in Figure 3.b and 3.e. As a result, the side chains are very well interdigitated.

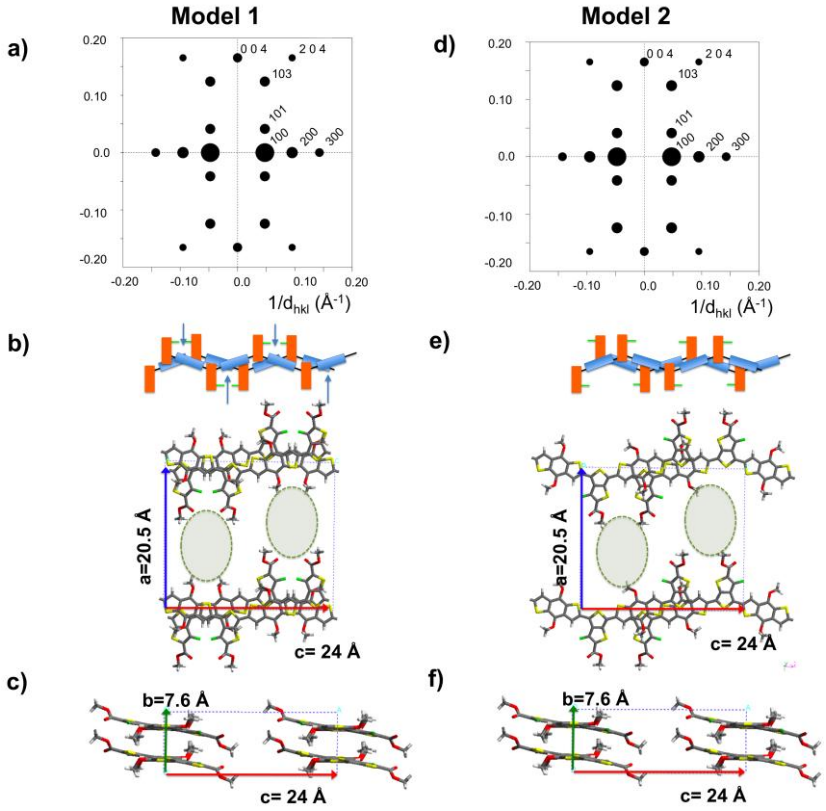

Figure 3*. Results of the structural modeling for PTB7 showing two possible structures labelled Model 1 (a-c) and Model 2 (d-f). In (a) and (d), the calculated [0 1 0] ED patterns for the models are shown. In (b) and (e), the models are shown in b-axis projection (π-stacking direction). In (c) and (f), the models are seen in c axis projection. For simplicity, the alkyl side chains are not shown but their location in the layered structure is indicated by dotted ellipses. A schematic illustration of the overlap between PTB7 chains is shown. The thieno[3,4-b]thiophene and benzodithiophene groups are represented in orange and blue respectively. The fluorine atom on the thieno[3,4-b]thiophene block is in light green. In (b), the blue arrows indicate the π-overlap between thiophene blocks of the benzodithiophene units in Model 1.*

Let us now compare the π-stacking of PTB7 backbones in both models. In Model 1, one entire thiophene cycle per benzodithiophene block is involved in a 3.8 Å π-overlap with the neighbouring thiophene of the underlying benzodithiophene block (blue arrows in Figure 3.b) but no other part of the conjugated backbone is involved in π-stacking with the neighbouring chain along **b**. The situation is different in Model 2. The π-overlaps are not limited to a precise thiophene cycle of the benzodithiophene but are more "delocalized" over the whole backbone of PTB7. Contrary to Model 1, no strong overlap between entire conjugated cycles exists in Model 2 (see Figure 3.e).

An alternative Model 3 with lower cell symmetry such as $P2_1$ was also identified. Successive π-stacked chains along **b** are no longer related by a 2_1 screw axis. Therefore, the structure is "polar" with respect to the chain orientation: all fluorine atoms of all π-stacked chains point in the same direction along the **c** axis. Figure S6 shows the refined structure of Model 3 corresponding to the best agreement with the experimental ED data, in effect very comparable to Model 1. This result suggests that the 2_1 screw axis along **b** may not be a necessary symmetry element in the structure. From a structural standpoint, Model 3 is similar to Model 1 in terms of π-overlaps between thiophene cycles of successive benzodithiophene blocks along the **b** axis and similar Δc shift between two π-stacked chains.

b) Comparing the stacking in PTB7 with other polymer semi-conductors.

It is interesting to compare the type of stacking evidenced in PTB7 with that observed for other representative alternated copolymers such as PCPDTBT, F-PCPDTBT or P(NDI2OD-T2) for which structural models have been proposed.[16,9] PCPDTBT and F-PCPDTBT both feature a segregated mode of stacking in the thermodynamically stable

form but the chains are paired in dimers with π-stacked backbones surrounded by alkyl side chains.[16] The case of P(NDI2OD-T2) is somewhat different. It has a characteristic polymorphism (form I and II) and long range π-stacking. In Form I, a segregated stacking of the naphthalenebisimide and bithiophene blocks exists whereas in the thermodynamically stable form II, a mixed stacking of the two blocks is observed.[9] In PTB7, the *all-cis* conformation of the monomers results in a marked zig-zag conformation of the chain whereas the previously mentioned polymers have a more linear backbone conformation. For the PTB7 zig-zag conformation, a perfect segregated stacking is sterically impeded by the branched alkyl side chains of the thieno[3,4-*b*]thiophene blocks. The presence of these side chains results in the Δc shifts of two successive π-stacked chains. Accordingly, this polymer illustrates the key role played by the alkyl side chain on the π-stacking of the conjugated backbone. It is also worth to note, that the zig-zag chain conformation adopted by PTB7 did not result in a cross-hatched packing of the chains as evidenced by Takacs *et al.* for Si-PCPDTBT.[28] One possible reason is that both thieno[3,4-*b*]thiophene and the benzodithiophene blocks bear branched alkyl side chains that impede the crossed-chain packing observed for Si-PCPDTBT.

3. Conclusions.

Highly oriented PTB7 thin films were obtained by high-temperature rubbing followed by thermal annealing. Three possible models for the stacking of PTB7 have been identified, based on the electron diffraction pattern of these oriented films. The films show high in-plane hole mobilities parallel to the rubbing direction and dichroic ratii of 12 in optical absorption. The films rubbed at T_R=200°C and annealed at T_A=260°C consist mainly of face-on crystals whereas edge-on crystals become dominant in films

rubbed at T_R=240°C and annealed at T_A=290°C. Structural modeling based on ED shows that, i) PTB7 chains form a "layered" packing similar to other PSCs such as PBTTT with π-stacked backbones alternating with layers of strongly interdigitated alkyl side chains, ii) the PTB7 chains adopt a non-planar zig-zag conformation, iii) PTB7 chains show a mixed stacking of thieno[3,4-*b*]thiophene and benzodithiophene blocks and iv) a shift Δc along the chain direction between two π-stacked chains results from sterical constraints imposed by the branched side chains of the thieno[3,4-*b*]thiophene blocks. This study shows that highly anisotropic properties of PTB7 can be achieved only under "extreme" processing conditions (high temperature rubbing and annealing at T≥ 260°C), possibly because of the zig-zag conformation of the polymer backbone cannot be reached when faster processing methods such as spin-coating or drop casting are used.

4. Experimental section.

a) Materials and thin film fabrication.

Poly[[4,8-bis[(2-ethylhexyl)oxy]benzo[1,2-*b*:4,5-*b*']dithiophene-2,6-diyl-[3-fluoro-2-[(2-ethylhexyl)carbonyl]thieno[3,4-*b*]thiophene-4,6-diyl]] (PTB7) was purchased from Solaris Chem. Inc. and used as received (M_n = 46 kDa, M_w = 87 kDa).

For TEM and UV-Vis studies, PTB7 films are prepared by doctor blading a 5 wt % solution in *ortho*-dichlorobenzene (*o*-DCB) or chloroform (CF) on clean glass slides (Roth) maintained at 170°C or 53°C, respectively. The solution in CF (o-DCB) were prepared by dissolving the polymer at 45°C (120°C) and stirring during 90 min. Cleaning of the glass substrates is described in the literature.[29] A film thickness of 15±5nm was determined from the absorbance at 695 nm and reference data from the literature.[30] For

GIXD experiments, PTB7 films were prepared on Si(100) wafers (Silchem). After cleaning the substrates and UV-Ozone treatment, the films were deposited by doctor-blading a 5 wt % solution in CF at 53°C.

Mechanical rubbing of PTB7 films was performed following the methodology described in our previous work.[12-15] In short, a microfiber cloth is applied at a pressure of 2.4 bar on the films. The so-called rubbing length is fixed at ca. 50 cm, rotation speed of the cylinder at 300 rpm and translation speed of the stage 5 mm/s. The rubbing temperature is varied from ambient to 200°C and three rubbing cycles are used. To avoid chemical degradation of the films, the rubbing was performed under N_2 atmosphere (plaslab glove box). Post-rubbing annealing was performed in a Linkam LTS420 hot stage under N_2 atmosphere.

b) Thin film characterization.

Polarized UV-vis absorption spectroscopy was performed using a Varian Carry 5000 UV-VIS-NIR spectrometer with polarized incident light. SEM observations were performed at 1kV with a HITACHI SU90 FEG-SEM on as-prepared OFET devices (no gold coating).

For TEM analysis, the PTB7 films were coated with a thin amorphous carbon film evaporated using an Auto 306 evaporator (Edwards). Oriented areas were identified for TEM analysis by Polarized Optical Microscopy (POM) (Leica DMR-X microscope). The samples are then removed from the glass substrate by the polyacrylic acid method, floated on water and recovered on TEM copper grids. TEM was performed in bright field (BF), high resolution (HRTEM) and electron diffraction (ED) modes using a CM12 Philips

microscope equipped with a MVIII (Soft Imaging System) Charge Coupled Device camera. Specific conditions for HR-TEM and low dose diffraction are given elsewhere.[31]

Grazing-incidence X-ray diffraction (GIXD) experiments were performed at BL9 beamline of the DELTA synchrotron radiation facility (Dortmund, Germany). This beamline is dedicated to small angle X-ray scattering and GIXD experiments. At BL9 beamline the footprint of the incoming X-ray beam has a typical size 0.2 x 1 mm^2 in horizontal and vertical directions, respectively. For GIXD measurements, the photon energy and the incidence angle α_i were set to 15 keV and 0.1°, respectively. 2D MAR345 image plate (3450×3450 pixels, resolution of 100 μm per pixel) detector was used to record the diffraction patterns. The angularly-resolved data were converted to reciprocal space where the axes of perpendicular ($q_\perp$) and parallel ($q_{//}$) components of the momentum transfer vector correspond to scattering along perpendicular (out-of-plane) and parallel (in-plane) directions, respectively. The orientation of the aligned films was chosen such that the incident X-ray beam q_i is oriented either parallel or perpendicular to the rubbing direction R.

Bottom-Gate Bottom-Contact (BG-BC) field-effect transistors (OFETs) were elaborated on pre-patterned test structures (Fraunhofer) the source and drain contacts of which were composed of a 30 nm thick gold layer on top of a 10 nm thick Indium Tin Oxide (ITO) layer. A 230 nm thick silicon oxide was used as gate dielectric and n-doped silicon crystal as gate electrode. The channel length and channel width are L=20 μm and W= 10 mm, respectively. These electrode patterns were oriented along two directions on the substrates at 90° relative orientation to each other so that charge transport could be measured both parallel and perpendicular to the rubbing direction. The transistor substrates were cleaned by sonication in hellmanex, water, acetone and isopropanol at

45°C for 15 min in each solvent. After drying under nitrogen, the substrates were exposed to an ultra-violet ozone atmosphere for 15 min. Surface functionalization of the SiO_2 was performed by depositing a thin layer of hexamethyldisilazane (HMDS) by spin coating, followed by thermal annealing of the substrates at 135°C. Polymer films of ~ 30 nm thickness were spin-coated from 5 wt % solutions in *CF* (1000 rpm for 30 s and then 1500 rpm for 60 s). The polymer solutions were prepared by dissolution at 55°C for 4 hrs under continuous stirring. After deposition, the samples were rubbed and then left under vacuum ($<10^{-6}$ mbar) overnight to remove residual solvent traces. All polymer solutions and films were prepared in a nitrogen atmosphere.

The charge transport properties characterization of the OFETs was carried out in a nitrogen atmosphere using a Keithley semiconductor parametric test system. The field-effect mobilities (μ_{FET}) were determined from the current-voltage transfer characteristics in the saturation regime using the following equation (1):

$$\mu_{sat}(V_g) = \frac{\partial I_{ds,sat}}{\partial V_g} \cdot \frac{L}{WC_i} \cdot \frac{1}{(V_g - V_{Th})} \quad (1)$$

where $I_{ds,sat}$ is the source-drain current, V_g is the gate voltage, V_{Th} is the threshold voltage, W is the channel width, L is the channel length and C_i is the capacitance per unit area of the gate dielectric.[32,33]

The mobility values were measured for both saturation mode and linear modes. 3-4 devices were used to measure mobilities and charge anisotropy for each condition. The reported values of mobilities are the mean arithmetic values and the error bars are calculated as the standard deviations of the obtained values.

c) Structural modeling.

The modeling of the structure of PTB7 followed the general approach described in reference for P3HT form I.[34] First, a trial-and-error approach was used to refine a first structural model of PTB7 that was not minimized in energy. This preliminary model helped determine a first backbone conformation that was used for the refinement by Density Functional Theory (DFT) calculations. To this end we have used the DFT localized orbital molecular dynamics technique Fireball.[35] This technique has already proven to give good results on molecular systems.[36,37] Starting from fluoride-thienothiophene and benzodithiophene molecules, we have built the fluoride-PTB7 molecular unit, and subsequently a fluoride-PTB7 tetramer. Standard *sp* optimized numerical basis sets have been used as described in ref. 36. Structural optimizations have been performed until forces reached values lower than 0.1 eV/Å. The obtained configurations are in good agreement with the previous measurements, since only very small configuration changes have occurred between the initial and the final molecular structures. A non-planar backbone conformation was obtained as proposed earlier by Bhatta et al. with a torsion angle between the benzodithiophene and the thienothiophene of approx. 20 deg.[25] This backbone conformation was then used in the modeling of the ED pattern to verify adequacy with the experimental ED pattern.

Supporting Information.

Supporting Information is available from the Wiley Online Library or from the author.

Acknowledgments.

B. Lotz is gratefully acknowledged for fruitful discussions and careful reading of the manuscript. L. Hermann and P. Allgayer are gratefully acknowledged for technical support in the design and fabrication of the rubbing machine. We are extremely grateful to the MaCEPV team at ICUBE (N. Zimmermann, P. Lévêque and T. Heiser) for technical support in charge transport measurements, privileged access to the glove box platform and fruitful discussions on charge transport measurements. L. Biniek thanks the Université de Strasbourg, the Investissements d'Avenir (IdEx Attractivité 2015) and the Région d'Alsace (Fédération de recherche Matériaux et Nanosciences Alsace AAP 2015) for financial supports. We are grateful for financial support from the DAAD-PROCOPE (project No. 57211900), the BMBF (project No. 05K13PS4) and BL9 beamline scientists for assistance at the DELTA synchrotron.

References.

(1) A. Salleo, *Materials Today* **2007**, *10*, 38.

(2) (a) M. Brinkmann and J.-C. Wittmann, *Adv. Mat* . **2006**, 16, 820. (b) M. Brinkmann, *J. Polym. Sci. Polym. Phys.* **2011**, *49*, 1218.

(3) D. Venkateshvaran, M. Nikolka, A. Sadhanala, V. Lemaur, M. Zelazny, M. Kepa, M. Hurhangee, A. J. Kronemeijer, V. Pecunia, I. Nasrallah, I. Romanov, K. Broch, I. McCulloch, D. Emin, Y. Olivier, J. Cornil, D. Beljonne and H. Sirringhaus *Nature*, **2014**, *515*, 348.

(4) E. J. W. Crossland, K. Tremel, F. Fischer, K. Rahimi, G. Reiter, U. Steiner and S. Ludwigs *Adv. Mater.***2012**, *24*, 839.

(5) J. Liu, J. Zou and L. Zhai, *Macromol. Rapid Commun.* **2009**, *30*, 1387.

(6) N. D. Treat, J. A. Nekuda Malik, O. Reid, L. Yu, C. G. Shuttle, G. Rumbles, C. J. Hawker, M. L. Chabinyc, P. Smith and N. Stingelin *Nat. Mater.* **2013**, *12*, 628.

(7) A. Hamidi-Sakr, D. Schiefer, S. Covindarassou, L. Biniek, M. Sommer, M. Brinkmann, *Macromolecules* **2016**, *49*, 3452.

(8) (a) M. Brinkmann, *Macromolecules* **2007**, 40, 7532. (b) M. Brinkmann, N. Charoenthai, R. Traiphol, P. Piyakulawat, J. Wlosnewski and U. Asawapirom, *Macromolecules* **2009**, *42*, 8298.

(9) M. Brinkmann, E. Gonthier, S. Bogen, K. Tremmel, S. Ludwigs, M. Hufnagel, M. Sommer, *ACS Nano* **2012**, *6*, 10319.

(10) M. Brinkmann, C. Contal, N. Kayunkid, T. Djuriç, R. Resel, *Macromolecules* **2010**, *43*, 7604.

(11) B. O'Connor, R. J. Kline, B. R. Conrad, L. J. Richter, D. Gundlach, M. F. Toney, D. M. DeLongchamp, *Adv. Funct. Mater.* **2011**, *21*, 3697.

(12) M. Brinkmann, L. Hartmann, L. Biniek, K. Tremel and N. Kayunkid, *Macromol. Rapid. Comm.* **2014**, *35*, 9.

(13) L. Biniek, S. Pouget, D. Djurado, E. Gonthier, K. Tremel, N. Kayunkid, E. Zaborova, N. Crespo-Monteiro, O. Boyron, N. Leclerc, S. Ludwigs and M. Brinkmann *Macromolecules* **2014**, *47*, 3871.

(14) L. Biniek, N. Leclerc, T. Heiser, R. Bechara, M. Brinkmann, *Macromolecules* **2013**, *46*, 4014.

(15) A. Hamidi-Sakr, L. Biniek, S. Fall, and M. Brinkmann, *Adv. Funct. Mater.* **2016**, *26*, 408.

(16) F. S. U. Fischer, N. Kayunkid, D. Trefz, S. Ludwigs and M. Brinkmann, *Macromolecules* **2015**, *48*, 3974 – 3982.

(17) S. B. Dkhil, M. Pfannmöller, S. Bals, T.Koganezawa, N.Yoshimoto, D. Hannani, M. Gaceur, C.Videlot-Ackermann, O. Margeat, and J. Ackermann, *Adv. Energy Mater.* **2016**, 1600290.

(18) Q. Wan, X. Guo, Z. Wang, W. Li, B. Guo, W. Ma, M. Zhang, and Y. Li, *Adv. Funct. Mater.* **2016**, *26*, 6635.

(19) L. Lu and L. Yu *Adv. Mater.* **2014**, *26*, 4413.

(20) W. Chen, T. Xu, F. He, W. Wang, C. Wang, J. Strzalk, Y. Liu, J. Wen, D. J. Miller, J. Chen, K. Hong, L. Yu, and S. B. Darling *Nano Lett.* **2011**, *11*, 3707.

(21) F. Liu, W. Zhao, J. R. Tumbleston, C. Wang, Y. Gu, D. Wang, A. L. Briseno, H. Ade and T. P. Russell, *Adv. Energy Mater.* **2014**, *4*, 1301377.

(22) S. Guo, E. M. Herzig, A. Naumann, G. Tainter, J. Perlich, P. Müller-Buschbaum, *J. Phys. Chem. B* **2014**, *118*, 344.

(23) M. R. Hammond, R. J. Kline, A. A. Herzing, L. J. Richter, D. S. Germack, H. W. Ro, C. L. Soles, D. A. Fischer, T. Xu, L. Yu, M. F. Toney, D. M. DeLongchamp, *ACS Nano* **2011**, *5*, 8248.

(24) J. M. Szarko, J. Guo, Y. Liang, B. Lee, B. S. Rolczynski, J. Strzalka, T. Xu, S. Loser, T. J. Marks, L. Yu, L. X. Chen, *Adv. Mater.* **2010**, *22*, 5468.

(25) R. S. Bhatta, D. S. Perry and M. Tsige, *J. Phys. Chem. A* **2013**, *117*, 12628.

(26) H. Xu, T. Xiao, J. Li, J. Mai, X. Lu, and N. Zhao *J. Phys. Chem. C* **2015**, *119*, 25598.

(27) K. Tremel, F. S. U. Fischer, N. Kayunkid, R. D. Pietro, R. Tkachov, A. Kiriy, D. Neher, S. Ludwigs, M. Brinkmann, *Adv. Energy Mater.* **2014**, *4* , 1301659.

(28) C. J. Takacs, M. A. Brady, N. D. Treat, E. J. Kramer and M. L. Chabinyc, *Nano Lett.* **2014**, *14*, 3096.

(29) M. Brinkmann, S. Graff, J.-C. Wittmann, C. Chaumont, F. Nuesch, A. Anver, M. Schaer and L. Zuppiroli *J. Phys. Chem. B* **2003**, *107*, 10531.

(30) L. Wang, S. Zhao, Z. Xu, J. Zhao, D. Huang and L. Zhao, *Materials* **2016**, *9*, 171.

(31) M. Brinkmann and P. Rannou, *Macromol*ecules **2009**, *42*, 1125.

(32) J. Zaumseil and H. Sirringhaus *Chem. Rev.* **2007**, *107*, 1296.

(33) H. Klauk, *Chem. Soc. Rev.* **2010**, *39*, 2643.

(34) N. Kayunkid, S. Uttiya and M. Brinkmann, *Macromolecules* **2010**, *43*, 4961.

(35) J. P. Lewis, P. Jelínek, J. Ortega, A. A. Demkov, D. G. Trabada, B. Haycock, H. Wang, G. Adams, J. K. Tomfohr, E. Abad, H. Wang, D. A. Drabold, *Physica Stat. Sol. B* **2011**, *248*, 1989.

(36) V. E. Campbell, M. Tonelli, I. Cimatti, J.-B. Moussy, L. Tortech, Y. J. Dappe, E. Rivière, R. Guillot, S. Delprat, R. Mattana, P. Seneor, P. Ohresser, F. Choueikani, E. Otero, F. Koprowiak, V. G. Chilkuri, N. Suaud, N. Guihéry, A. Galtayries, F. Miserque, M.-A Arrio, P. Sainctavit and T. Mallah, T. *Nature Comm.* **2016**, *7*, 13646.

(37) M. A. Basanta, Y. J. Dappe, P. Jelinek and José Ortega, *Computational Materials Science* **2007**, *39*, 759.